ACS APPLIED MATERIALS & INTERFACES

Research Article

www.acsami.org

First-Principles Analysis of Defect-Mediated Li Adsorption on Graphene

Handan Yildirim,[†] Alper Kinaci,[‡] Zhi-Jian Zhao,[†] Maria K. Y. Chan,[‡] and Jeffrey P. Greeley*,[†]

[†]School of Chemical Engineering, Purdue University, West Lafayette, Indiana 47907, United States

[‡]Center for Nanoscale Materials, Argonne National Laboratory, Argonne, Illinois 60439, United States

Supporting Information

ABSTRACT: To evaluate the possible utility of single layer graphene for applications in Li ion batteries, an extensive series of periodic density functional theory (DFT) calculations are performed on graphene sheets with both point and extended defects for a wide range of lithium coverages. Consistent with recent reports, it is found that Li adsorption on defect-free single layer graphene is not thermodynamically favorable compared to bulk metallic Li. However, graphene surfaces activated by defects are generally found to bind Li more strongly, and the interaction strength is sensitive to both the nature of the defects and their densities. Double vacancy defects are found to have much stronger interactions with Li as compared to Stone−Wales defects, and increasing defect density also enhances the interaction of the Stone−Wales defects with Li. Li interaction with one-dimensional extended defects on graphene is additionally found to be strong and leads to increased Li adsorption. A rigorous thermodynamic analysis of these data establishes the theoretical Li storage capacities of the defected graphene structures. In some cases, these capacities are found to approach, although not exceed, those of graphite. The results provide new insights into the fundamental physics of adsorbate interactions with graphene defects and suggest that careful defect engineering of graphene might, ultimately, provide anode electrodes of suitable capacity for lithium ion battery applications.

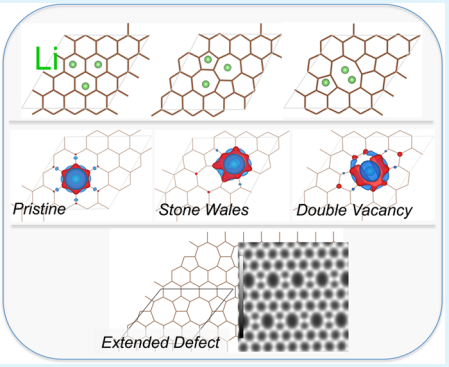

KEYWORDS: *lithium ion battery, graphene, defects, density functional theory, van der Waals interactions, genetic algorithm*

1. INTRODUCTION

Rechargeable Li ion batteries (LIBs) are indispensable for energy storage in applications ranging from portable electronics to electric vehicles.[1−4] Although such batteries are widely used, the search for higher energy density electrodes remains a topic of intense study.[1−4] In most commercial LIBs, carbon-based materials,[5−7] including graphite and modified graphite,[8,9] have been utilized as anode materials even though the capacity of graphite is limited to 372 mAh/g.[5] Given this modest capacity, the choice of graphite anodes in commercial applications stems primarily from the facts that they are durable and that dendrite formation can be controlled.[10]

Motivated by a desire to replace graphite anodes with a higher capacity alternative, nanomaterials have attracted much attention, as they are expected to have high storage capacities due to their high surface-to-mass ratios. Recently, an allotrope of carbon, graphene,[11,12] a single layer of honeycomb-structured carbon atoms, has been explored as an alternative to graphite. Its outstanding mechanical strength and electronic conductivity, together with its known hydrogen storage capacity[13] and ready availability of extra storage sites, which may possibly lead to a higher capacity than graphite,[14−16] suggest that it may have promising storage properties.[17,18] In addition, because graphene has been explored as a conducting additive to active materials in electrodes,[19−21] and because the flexibility and high fracture strength of graphene may provide enhanced battery cycle life,[22] understanding the Li−graphene interaction is also relevant for determining the properties of hybrid electrode materials.

Some experimental studies have shown that graphene nanosheets and oxidized graphene nanoribbons can absorb more Li than graphite.[16,23] For instance, it was reported that disordered graphene sheets can have reversible capacities of 794−1054 mAh/g.[23] Furthermore, other experimental[24,25] and computational[26−30] studies predicted that graphene can absorb Li ions through a specialized Li ordering on both of its sides, resulting in a higher theoretical capacity than that of graphite. Close examination of these and related graphene samples suggested that the Li storage capability could be attributed to the binding of Li with defects formed during the fabrication of the nanosheets.[23,31] On the other hand, an experimental study based on *in situ* Raman spectroscopy by Pollak et al.[32] showed less promising results for Li capacity than these other studies. It was reported that the amount of Li absorbed on single layer graphene (SLG) is significantly lower than that on graphite, while intercalation into few layer graphene (FLG) resembled that of graphite.[32] Moreover, on the basis of the cluster expansion method and density functional theory (DFT)

Received: September 4, 2014
Accepted: November 14, 2014
Published: November 14, 2014

   dx.doi.org/10.1021/am506008w | ACS Appl. Mater. Interfaces 2014, 6, 21141−21150

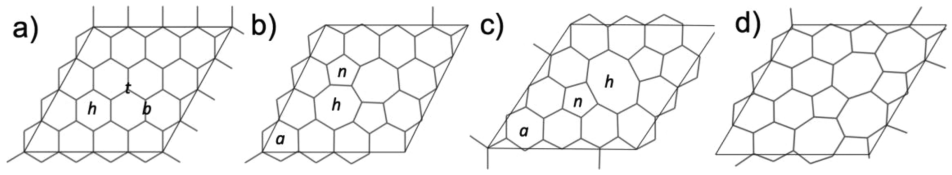

Figure 1. Schematic views of graphene structures for (a) pristine graphene, (b) graphene with one Stone-Wales (SW) defect, (c) graphene with one double vacancy (DV) defect, and (d) graphene with two SW defects. The computational cell is represented by the parallelogram. The letters t, b, and h indicate top, bridge, and hollow site configurations of Li, respectively, whereas the letters n and a indicate the near-defect and far-from defect Li adsorption sites, respectively.

calculations,[33] it was predicted that there are no Li arrangements that stabilize Li absorption on pristine SLG relative to bulk metallic Li. Thus, the authors of ref 33 concluded that defect-free SLG has significantly lower capacity than graphite, and they hypothesized that the experimentally reported capacities for SLG, ranging from Li_2C_6 to $Li_{0.3}C_6$,[16,24,25,32] result from existing defective microstructures and from Li absorption on the edges of the graphene sheets.[33]

Several computational studies have examined the adsorption properties of isolated Li or a single layer of Li adatoms on pristine graphene, and bonding and charge transfer in these structures have been analyzed.[34−37] A common observation from these studies[34−37] is that the Li ion is stabilized in the center of the carbon ring, where six carbon atoms interact with Li, with weaker adsorption at the bridge site and top sites.[28] The binding is reported to be ionic in nature with charge transferred from the Li to the graphene.[28,29] A recent DFT study[38] also reported Li adsorption on defect-free SLG with van der Waals (vdW) interactions (using the DFT-D2 method), concluding that Li binds more weakly to the defect-free SLG than to graphite. The authors found that small Li clusters are formed on the graphene with increased Li coverage, and they speculated that formation of clusters raises concerns about the stability of the anode against dendrite formation and that the use of graphene as an anode is unlikely to increase the capacity unless the surface of graphene is modified.

These experimental and computational studies point to the importance of studying the effect of defects in graphene on Li adsorption. In spite of these motivations, however, only a few computational studies have been carried out on the adsorption and diffusion of Li atoms on graphene with defects; we note that all of these studies focused exclusively on the adsorption properties of isolated Li atoms on graphene.[39−43] One such study[39] reported the adsorption and diffusion of Li on graphene with a single vacancy (SV) defect, concluding that a vacancy has the tendency to capture Li and that the barrier for Li penetration through graphene with a SV defect is as high as that through pristine graphene. A DFT study also reported that Li penetration is facilitated by defects, and double vacancy (DV) and higher order defects have reasonable barriers that allow Li diffusion through the basal plane. However, the barrier is high for both SV and Stone−Wales (SW) defects.[42] Additional DFT studies[42,43] showed that the presence of vacancy defects can increase the magnitude of the adsorption energy near the defect region, and Li can diffuse through the double vacancy (DV) defect with a smaller barrier compared to the corresponding barriers on pristine graphene and graphene with SV defects.[43] These results suggest that,[42] in the presence of DV and higher order defects, Li adsorption on, and penetration through, graphene can be enhanced. Finally, a recent DFT study evaluated the feasibility of Li storage in graphene and its derivatives, demonstrating that certain structural defects can bind Li stably and that doping with boron is also an effective strategy to enhance Li binding.[44]

Several experimental studies have elucidated the atomistic structure of both intrinsic and physically introduced defects in graphene. For instance, transmission electron microscopy (TEM)[45−48] and scanning tunneling microscopy (STM)[49,50] experiments have revealed images of graphene with point, as well as extended, defects[51] with atomic resolution. The high formation energies of point defects, including SW and DV defects, imply that they would be present at low concentrations in thermal equilibrium at temperatures below melting. However, we note that, in spite of these thermodynamic barriers, three mechanisms could lead to higher concentrations of defects in graphene: (i) nonequilibrium crystal growth, (ii) irradiation with energetic particles,[52] and (iii) chemical treatment. It is these nonequilibrium structures that are the primary focus of the present work.

In the present study, we perform first principles calculations of Li adsorption on pristine SLG, graphene with SW and DV point defects of varying densities, and an extended defect consisting of two octagons connected with a pair of pentagons,[51] to explore the feasibility of modifying graphene to store additional Li. Using a variety of search techniques, including a genetic algorithm (GA), we identify the lowest energy structures of various defects, the stable adsorption configurations for Li at varying Li coverages on SLG with different densities of SW and DV defects, and Li configurations on SLG with the extended defect. We demonstrate that defects can substantially enhance the amount of Li that can be accommodated on the graphene surfaces. However, we find that even for fairly high densities of defects (corresponding to mean distances between defects of 4.5 and 4.8 Å for DV and SW defects, respectively), Li capacities are still below that offered by graphite. We also find that the Li capacity of graphene with an extended defect exceeds that of bilayer graphene but is nonetheless below that of graphite. These analyses provide insight into the role of defect types, as well as their densities, on Li adsorption and storage, thus providing potentially useful input for the design of alternative electrode structures for energy storage.

2. COMPUTATIONAL DETAILS

DFT calculations are performed with the projector augmented wave (PAW) potentials as implemented in the Vienna Ab-intio Simulation Package (VASP).[53,54] The generalized gradient approximation (GGA) with the parametrization of Perdew−Burke−Ernzerhof (PBE)[55] is used for the exchange correlation energy of interacting electrons. We tested the total energy convergence for 300−600 eV planewave cutoffs with k-point sampling of 3 × 3 × 1, 6 × 6 × 1, and 9 × 9 × 1 Monkhorst-Pack grids. The differences in the total energies are less than 1 meV/atom for the 500 eV cutoff with the 6 × 6 × 1 k-point grid in comparison with the 9 × 9 × 1 grid, and the total energies are seen to be converged to 2 meV/atom with respect to planewave cutoff.

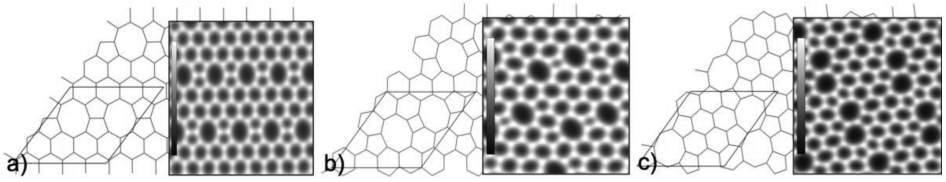

Figure 2. Schematic representation of high density DV defect configurations predicted using a genetic algorithm method for (a) an extended defect, and (b,c) DV point defects. The inset figures represent the charge density contour plots of the chosen plane parallel to the surface of the graphene.

Thus, the calculations are performed using a kinetic energy cutoff of 500 eV for the plane wave expansion, and the Brillouin zone of the 32-atom supercell is sampled with the Γ-centered k-point grid of 6 × 6 × 1. Spin-polarized calculations are performed to account for possible magnetism of defected graphene structures.

We use a supercell consisting of a single layer of pristine graphene with by 4 × 4 primitive cells (see Figure 1a) and 20 Å vacuum spacing. The creation of SW defects involves an in-plane 90° rotation of two C atoms with respect to the midpoint of the bond.[56] Following this transformation, four of the hexagons are replaced with two heptagons and two pentagons, as shown in Figure 1b. To increase the density of the defects, using the same computational cell, we apply an additional in-plane 90° rotation of two C atoms. For the DV defect, we remove two C atoms from the cell; by doing so, one DV defect is created in the cell (see Figure 1c). This process is followed by the removal of the second set of two C atoms to increase the density of the defect. After the defects are created, the structures are relaxed with modulation of the lattice parameters, and the positions of atoms are fully optimized. The changes in the lattice constants caused by defects are presented in the Supporting Information. We also run additional simulations using the GA to determine the most stable high density DV defect structures.

For successive Li adsorption on the graphene, we start with the lowest energy adsorption configuration of single Li for each structure (determined by a scan of the potential energy surface (PES)), and we then introduce the next Li to the sites at which the Li−Li distance is at least 3.0 Å (determined by additional scans of the PES for high Li content). For all possible sites found for Li, we optimize the structures, and we evaluate the associated total energies. The resulting total energies are classified from the lowest to highest, and we choose the lowest energy structure for further Li adsorption. For each Li concentration, we consider both single-sided and double-sided adsorption configurations. The lowest energy configurations resulting from this lithiation procedure are presented in Figures S2 and S3 in the Supporting Information, along with a comparison to the structures generated by the genetic algorithm. The GA, in turn, starts with an initial generation for which a population of 20 members is selected. The Li positions are randomly generated with predefined Li−Li and Li−C distances. The structures are relaxed, and after each generation, the most stable systems are selected for generating the offspring by mating. Further details regarding the method are summarized in the Supporting Information. The structural analyses suggest that for all Li coverages considered, Li is always found to relax to the hollow site.

For evaluating the effect of vdW interactions on the strength of Li adsorption on SLG, dispersion corrections are introduced using several approaches, including the correction scheme of Grimme (DFT-D2),[57] with default and modified dispersion coefficients for Li, and DFT-D3,[58] which adds a semiempirical pairwise force field to conventional DFT calculations. Additionally, to further assess the results obtained with these approaches, the calculations are repeated using the vdW-DF2,[59] as well as the vdW-DF family of functionals of optPBE-vdW,[60] optB88-vdW,[60] and optB86b-vdW,[61] which add a nonlocal correlation functional that approximately accounts for dispersion interactions. For isolated Li atoms, the contribution of the vdW interactions to the Li adsorption energy is evaluated with the above functionals at a variety of Li-graphene distances, and the resulting one-dimensional energy scans are reported. For the higher Li contents discussed later in the text, we restrict our analysis to PBE-optimized lowest energy adsorption geometries and reoptimize these configurations with the DFT-D2, DFT-D3, and vdW-DF2 functionals. To test whether the lowest energy configurations determined by PBE at a given coverage are consistent with the corresponding lowest energy geometries of these other functionals, we recalculated all adsorption geometries with the vdW-DF2 approach; the ordering of energies did not change between PBE and vdW-DF2.

3. RESULTS AND DISCUSSION

Structures of Graphene with Defects. We start with pristine SLG for which a 4 × 4 supercell is used as a model (Figure 1a). We then introduce point defects (SW and DV) on graphene at both low (one defect per 4 × 4 cell, Figure 1b,c) and high (two defects per 4 × 4 cell, Figures 1d and 2) density, as well as an extended defect on graphene (Figure 2a). The extended defect considered on graphene is basically made of point defects as building blocks, consisting of two octagons, which are connected by a pair of pentagons (Figure 2a).[51] Such a defect configuration has been suggested to act as a metallic wire embedded into a hexagonal lattice and is highly conducting.[51] The defect formation energies are determined from the formula $E_{form} = E_{def} - N\mu(C)$, where E_{def} is the total energy of the graphene with defect, N is the number of atoms in the graphene with defect, and $\mu(C)$ is the chemical potential of C, which is given by the total energy of pristine graphene divided by the number of C atoms.

The defect formation energies of low density defects, i.e., with one defect per 4 × 4 cell, are 4.0 and 6.2 eV for SW (Figure 1b) and DV (Figure 1c) structures, respectively. The formation energies are, in general, less positive than those reported in the literature (4.8−5.22 eV for SW and 7.02−8.0 eV for DV),[62−64] possibly because of the larger cell sizes (48−148 atoms), the use of different exchange correlation functionals, or the absence of unit cell relaxation in the indicated efforts. In these other studies, the cell sizes are large and the cell volumes are fixed in order to simulate isolated defects, whereas in our calculations, the cell volumes are relaxed and smaller cell sizes are employed to simulate higher defect densities. In the Supporting Information, we report on test calculations where we show that larger unit cells, and neglect of unit cell relaxation, do indeed increase the calculated formation energies of defects into the approximate range reported above. However, although these changes are not negligible, we emphasize that the adsorption energies of Li on defects, which will be the primary determinant of voltages in Li ion battery applications, do not change dramatically as a function of unit cell size (~50 meV between relaxed (4 × 4) and (5 × 5) unit cells on isolated double vacancy defects).

To generate a higher density SW defect configuration, we began with the already optimized low density SW defect configuration (one defect in a 4 × 4 cell), and then systematically rotated all available C−C bonds; the resulting lowest energy configuration is shown in Figure 1d, and the average formation energy is 4.34 eV. To determine the lowest

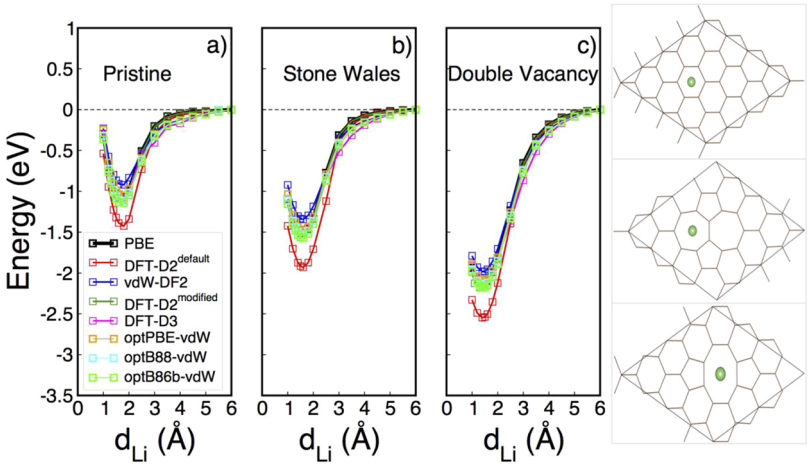

Figure 3. Potential energy surfaces of Li approaching the graphene surfaces evaluated using both PBE and vdW interactions for (a) pristine graphene, (b) SW defect, and (c) DV defect. The schematic representations of the associated Li adsorption configurations (on the h sites) are shown on the right. Note that the reference state is not bulk Li for these potential energy scans; the zero of the energy is referenced to the total energies associated with Li being farthest away from the graphene surfaces.

energy configurations corresponding to high density DV defects (two defects per 4 × 4 cell), we perform calculations using a GA method. The generation of the high density DV defect configurations using the GA proceeds, at the first step, by optimizing only the in-plane positions of C atoms and is followed by complete optimization of all C atoms in the cell when the lowest energy structures are found with the GA. Further details of the GA are given in the Computational Details section and in the Supporting Information.

In Figure 2, three high density defect configurations predicted by the GA are shown in order of decreasing stability. The predicted lowest energy configuration is an extended defect at which two octagons are connected by a pair of pentagons (see Figure 2a). Such an extended defect configuration has recently been observed experimentally with atomic resolution using STM for CVD-grown graphene on Ni(111).[51] Following this extended defect configuration, the second lowest energy configuration predicted by the GA corresponds to that of a linear arrangement of DV defects in which two octagons are connected by a C tetragon (Figure 2b). This configuration has also been observed experimentally with atomic resolution using TEM.[48] Finally, the least stable structure is shown in Figure 2c, where the two octagons are directly connected to each other. The corresponding average formation energies of these high density defect structures are 4.7, 6.0, and 7.0 eV, respectively.

We note, in passing, that in a real anode, where multiple layers of defected graphene might be present, a modest additional driving force for binding between graphene sheets might be present. However, test calculations show that the equilibrium spacing between graphene sheets changes by less than 0.5% with the introduction of DV defects. Thus, we do not expect these effects to dominate the behavior of the system. On the other hand, the changes in Li binding energies due to the presence of defects will likely be more significant.

Single Li Adsorption on Graphene with and without Defects. Lee et al.[33] reported that Li does not have favorable adsorption energetics (relative to bulk metallic Li) on defect-free SLG, making it unsuitable as an anode for LIBs. Although both SLG and FLG provide more surface area for Li adsorption, the weak Li binding leads to reduced capacity compared to that offered by graphite.[33,44] As mentioned above, one of the possible strategies to overcome this problem is to activate the surface of graphene with defects. Below, we report results for Li adsorption on both defect-free and defected graphene surfaces, beginning with GGA-PBE calculations and later briefly discussing how these results vary with the inclusion of dispersion corrections.

We start by describing Li adsorption on defect-free SLG. The lowest energy adsorption configuration of isolated Li, evaluated at the hollow (h), bridge (b), and top (t) sites (see Figure 1a), is found to be the hollow site in which Li binds to six C atoms. At this site, the Li distance to the graphene surface is 1.72 Å with a Li−C bond length of 2.24 Å (PBE), in agreement with earlier studies, which used varying methods as well as cell sizes.[26,28,29,35−37] Our calculations demonstrate that Li does not adsorb ($E > 0$) on defect-free SLG using the metallic Li in the bcc phase as the reference, and this is also in agreement with recent reports.[33,44] On the other hand, when a reference of isolated Li atoms in the gas phase is used, the adsorption becomes exothermic (−1.16 eV). These conclusions are not modified with the inclusion of vdW interactions using DFT-D2,[57] DFT-D3,[58] and vdW-DF2[59] (see also discussion below).

For Li adsorption on SLG with low density SW and DV defects (Figures 1b,c), we find the lowest energy adsorption configurations on both types of defects to be the hollow sites ("h" in Figure 1b,c). The next most stable Li configuration in both structures is the near defect site (n), and the least stable structure (a) is farther away from the defect zone. The Li adsorption energies on graphene with the DV defect, obtained using PBE, at the n and a sites are 150 and 390 meV less stable compared to that on the h site, respectively, while for the SW defect, the corresponding differences are 70 and 200 meV. For the SW defect, we find that at the h site, the Li distance to the graphene is 1.59 Å, with the bond lengths to the underlying C atoms being 2.21 and 2.34 Å. For the DV defect, Li is 1.43 Å away from the graphene with bond lengths of 2.26 and 2.59 Å to the C atoms in the defect region. The Li adsorption energies, obtained using PBE, indicate that Li does not adsorb (E = 0.03 eV) on the graphene with low density SW defects, as is the case with pristine graphene, while Li adsorbs on the graphene with low density DV defects with adsorption energy of −0.71 eV

(−0.76 eV for the 5 × 5 cell). The difference in the Li interaction strength between the two types of defected graphene suggests that a low density SW defect does not affect Li binding with the graphene, whereas the presence of one DV defect has a more pronounced effect. Later, we discuss how these conclusions are affected by increases in defect density.

The Effect of vdW Interactions on Isolated Li Adsorption on Pristine and Defected Graphene. To assess the effect of vdW interactions on the Li adsorption energies, we employ the DFT-D2 method with the default Li C_6 dispersion coefficient (expressed hereafter as DFT-D2^{default}),[57] which has been suggested to be successful in describing graphene-based structures.[65] Additionally, the vdW interactions are evaluated using the DFT-D2[57] method with a modified Li dispersion coefficient (0.01 instead of the default value of 1.61) as reported in ref 47 (denoted here on as DFT-D2^{modifed}), with DFT-D3,[58] with vdW-DF2,[59] and with the vdW-DF family of functionals, including optPBE-vdW,[60] optB88-vdW,[60] and optB86b-vdW,[61] which add a nonlocal correlation functional that approximately accounts for dispersion interactions.

The results, summarized in Figure 3a−c, show that the vdW interactions introduced by the empirical scheme (DFT-D2^{default}) make a noticeable contribution to the strength of Li adsorption on both pristine and defected graphene, while the results for other functionals, including PBE, are relatively similar. The adsorption energies calculated using the metallic Li as the reference with PBE and with the inclusion of vdW interactions are summarized in Table 1. The contribution from the vdW interactions to the adsorption energy using the DFT-D2^{default} method is about 0.35−0.40 eV/Li. In contrast, by employing the DFT-D2 ^{modifed} method, Li binding energies are found to be very similar than those obtained using PBE. Using a similar approach for accounting the dispersion, the DFT-D3[58] method with PBE-relaxed geometries predicts slightly weaker binding energies to those obtained using PBE. The vdW-DF2 method predicts very similar binding energies as compared to those obtained using PBE. Overall, the vdW-DF functionals, on the other hand, predict slightly stronger Li binding as compared to PBE, with the largest deviation being about 100 meV. In general, the similarity of the results of most of the vdW-corrected approaches to one another and to the predictions from PBE suggest that, in contrast to systems involving graphite or FLG,[33,44] Li interaction with SLG is not highly sensitive to dispersion effects. This result may be related to the fact that the Li-graphene bond involves significant charge transfer and is substantially ionic (see discussion below), rendering weak dispersion interactions less significant. Motivated by these results, our subsequent discussions will refer primarily to PBE results.

Table 1. Comparisons of Li Adsorption Energies (eV) Calculated Using PBE and with the Inclusion of vdW Interactions[a]

functionals	Li/pristine	Li/SW	Li/DV
PBE	0.40	0.03	−0.71
DFT-D2^{default}	0.20	−0.28	−1.01
DFT-D2^{modified}	0.42	0.00	−0.74
DFT-D3	0.50	0.09	−0.63
vdW-DF2	0.42	0.04	−0.72
optPBE-vdW	0.41	0.00	−0.76
optB88-vdW	0.33	−0.03	−0.84
optB86b-vdW	0.35	−0.07	−0.82

[a]The reference energy for deriving adsorption energies is bulk Li.

We note that the predictions from DFT-D2^{default}, with dispersion coefficients that are not adjusted to account for different chemical environments,[66] deviate substantially from the predictions of any of the other functionals, and these results appear to show significant overbinding; similar results have been observed by Persson and co-workers.[33] They showed that when the default Li C_6 coefficients were used, they failed to predict trends in the intercalation energies.[33] More promisingly, calibrating the C_6 coefficient for Li was shown to accurately predict the stage formation and voltage profile as a function of Li concentration.

Charge Redistribution due to Isolated Li Adsorption on Pristine and Defected Graphene. To probe the electronic details of Li bonding with graphene, we evaluate charge redistribution resulting from the adsorption of Li on graphene using the charge density differences defined as $\Delta\rho(r) = \rho_{Li\text{-}G}(r) - [\rho_{Li}(r) + \rho_G(r)]$, where $\rho_{Li\text{-}G}(r)$, $\rho_G(r)$, and $\rho_{Li}(r)$ are the real-space electronic charge distribution of the Li-adsorbed graphene, isolated Li, and the Li-free graphene, respectively. As seen from Figure 4a−f, in all cases, charge is transferred from Li to the more electronegative C atoms, as evidenced by the blue region representing charge depletion. The transferred charge remains in the region between Li and the nearest neighbor C atoms, shown by the red regions representing charge accumulation. As a result, the electron

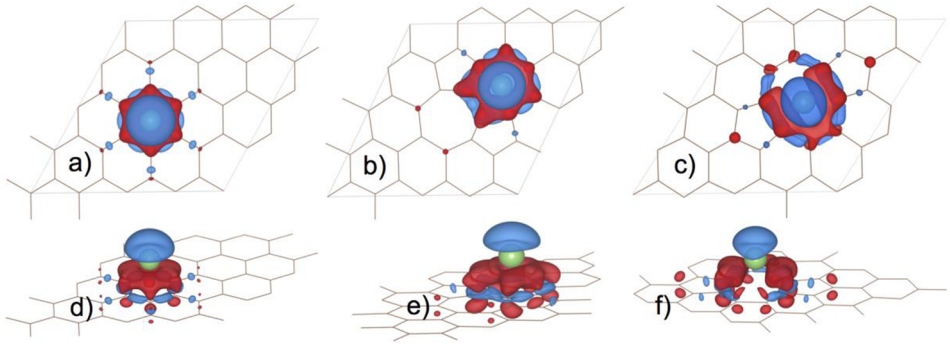

Figure 4. Top and side views of the calculated charge density difference for Li in the lowest energy adsorption configurations on graphene for (a,d) pristine graphene, (b,e) SW defect, and (c,f) DV defects. The isovalue for rendering the isosurfaces is 2.5×10^{-3} e/Å^3. The results are obtained using PBE. Blue and red represents negative and positive charge density differences, respectively.

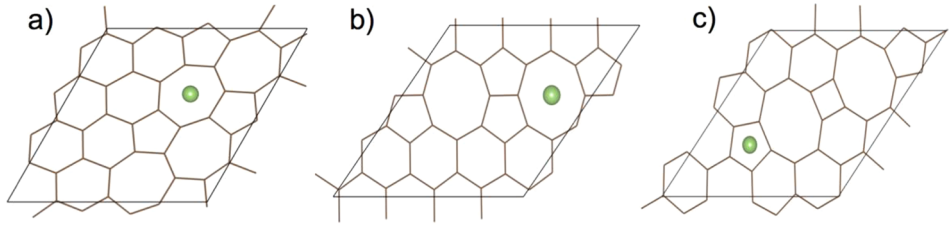

Figure 5. Schematic views of the lowest energy adsorption configurations for isolated Li on graphene structures with high defect densities for (a) SW defects, (b) a one-dimensional extended defect, and (c) DV defects.

density is reduced at the in-plane C−C bonds. The charge accumulation reduces the effective size of the hexagonal hole for pristine graphene, perhaps partly explaining the difficulty of Li penetration through this surface.[40,41]

For graphene with SW defects, we observe qualitatively similar features, while we note in the case of DV defects that the accumulation of charge density under the Li ion is noticeably less than that on both the pristine graphene and graphene with SW defects. This reduction in the density below Li may facilitate Li diffusion through graphene, leading to significantly lower diffusion barriers.[43] We also estimated the transferred charge to the graphene structures using Bader charge analysis.[67] Based on this approximate technique for charge estimation, the amount of charge transferred is ∼0.9 |e| for all graphene structures. This result is similar to the result reported in an earlier PBE study for Li adsorbed on pristine graphene, 0.89−1.0 |e|.[36]

Isolated Li Adsorption on Graphene with Increased Defect Densities. As described above, when using bulk bcc Li as the reference, there is no thermodynamically favorable adsorption of Li on either pristine graphene or on graphene with low density SW defects, while exothermic binding is observed on low density DV defects. We now analyze the effect of increased defect densities on Li adsorption energies. Figure 5a−c depicts the lowest energy adsorption configurations for Li on graphene with high density SW and DV defects (two defects in a 4 × 4 cell, Figures 1d and 2b, respectively), as well as on the extended defect (same average density as the high density DV defect) described above (Figure 2a). For the SW defect, we find Li to be stabilized at the hollow site above the heptagon (Figure 5a). For the one-dimensional extended defect containing two octagons connected by pair pentagons, the most stable adsorption site is the hollow site on top of the octagon (Figure 5b). On the other hand, for the less stable high density DV defect configuration in which the octagons are connected by a tetragon, Li is stabilized in the middle of the pentagon (Figure 5c).

Table 2 summarizes the Li adsorption energies obtained using PBE (Figure 5a−c). As compared to the low density SW defect case, in which Li adsorption is not possible ($E > 0$), increasing the defect density leads to more thermodynamically favorable adsorption of Li, suggesting that certain types of engineered higher density defect structures can enhance the interaction of Li with graphene. In addition, although Li adsorption is slightly less strong (60 meV) on the extended defects as compared to the low defect density case (Tables 1 and 2), we note that, with increasing Li content, the readily available additional octagon site for Li adsorption leads to more Li storage on this extended defect configuration, as discussed further below.

Table 2. Comparisons of Li Adsorption Energies (eV) at the Lowest Adsorption Energy Configurations on High Defect Density Graphene Structures and on an Extended Defect

functional	Li/SW defect	Li/DV defect	Li/extended defect
PBE	−0.46	−0.55	−0.65

Varying Li Concentrations on Graphene with Increased Defect Densities. We now turn to a discussion of the adsorption of Li on graphene structures with higher Li coverages. As discussed above, extensive test calculations, as well as analysis based on the GA, shows that hollow sites are the most favorable positions for Li on all the graphene structures for all coverages considered in this study (see Figures S2 and S3, Supporting Information). For insertion of successive Li atoms, we evaluate adsorption on the hollow sites in both single-sided and double-sided adsorption configurations (see Figure S4, Supporting Information for configurations on pristine graphene and on low defect density cases, and Figure S5, Supporting Information for charge density distributions of the selected configurations). In general, for all Li coverages on all graphene structures, we find the double-sided adsorption configurations to be more stable than the corresponding single-sided geometries.

To assess the amount of Li that can be favorably adsorbed on graphene with increasing Li coverage, we evaluate the differential binding energy, defined as $E_{\mathrm{bind}}^{\mathrm{diff}} = E_{n\mathrm{Li/G}} - E_{(n-1)\mathrm{Li/G}} - \mathrm{E}_{\mathrm{Li}}^{\mathrm{metallic}}$. Increasing Li coverage results in less favorable Li adsorption due to increasing Coulomb repulsion between the positively charged Li ions, as this repulsion is not screened as efficiently as in the case of the Li−graphite system.[44] We note that in graphite, the C atoms in successive graphene layers are bonded by vdW interactions. With Li intercalation, the interlayer C−C vdW forces decrease, and Li−Li repulsion increases. The balance between these interactions determines the critical Li concentration for which there is a sufficient thermodynamic driving force to populate empty layers. It was shown in an earlier DFT study that adding vdW corrections improves the phase sequence with increasing Li content as compared to experiment (ref 68, references therein) and that the effect of vdW interactions for Li intercalation into few layer graphene and bulk graphite is likely a function of the Li content as well as the number of graphene layers stacked together.[33] Hence, inclusion of vdW corrections is substantially more important when modeling graphite than it is for the single layer graphene systems considered here. In the case of SLG, the differential binding energies suggest that increasing defect density causes adsorption of Li to be thermodynamically favorable, permitting up to two Li (three Li for the extended defect in the 4 × 4 supercell) to be stably adsorbed (see Table 3).

Table 3. Differential Binding Energies[a] (eV) as a Function of Li Content

E_{bind}^{diff}	Li/SW low density	Li/SW high density	Li/DV low density	Li/DV high density	Li/DV extended defect
1Li	0.03	−0.46	−0.71	−0.55	−0.65
2Li	−0.03	−0.35	−0.42	−0.05	−0.45
3Li	0.50	0.28	0.55	0.35	−0.10

[a]Defined as $E_{bind}^{diff} = E_{nLi/G} - E_{(n-1)Li/G} - E_{metallic}^{Li}$ and calculated using PBE. The corresponding defect structures in the 4 × 4 supercell are shown in Figures 1b, 1d, 1c, 2b, and 2a, respectively.

The effect of Li coverage on the stability and Li capacity can also be analyzed through construction of convex hulls. The lithiation energy, or formation energy,[69] defined as $E_a(x) = [E(Li_xC) - xE(Li_{metallic}) - E(C)]/N$, is calculated using the DFT-determined total energies of the configurations at varying Li compositions with PBE and vdW functionals (see the Computational Details section for more information). $E(Li_xC)$ denotes the energy of a lithiated configuration, $E(C)$ is the energy of the graphene without Li, $E(Li_{metallic})$ is the energy of metallic Li bcc phase, and N is the number of C atoms in the graphene. The Li formation energies on graphene surfaces containing both low and high density SW and DV point defects are presented in Figure 6a–d, and the results for the extended defect are shown in Figure 7 below. All calculated lithiated configurations, including those that are higher in energy at each respective Li composition, are shown for PBE, but we report only the lowest energy configurations at a given composition for the other functionals.

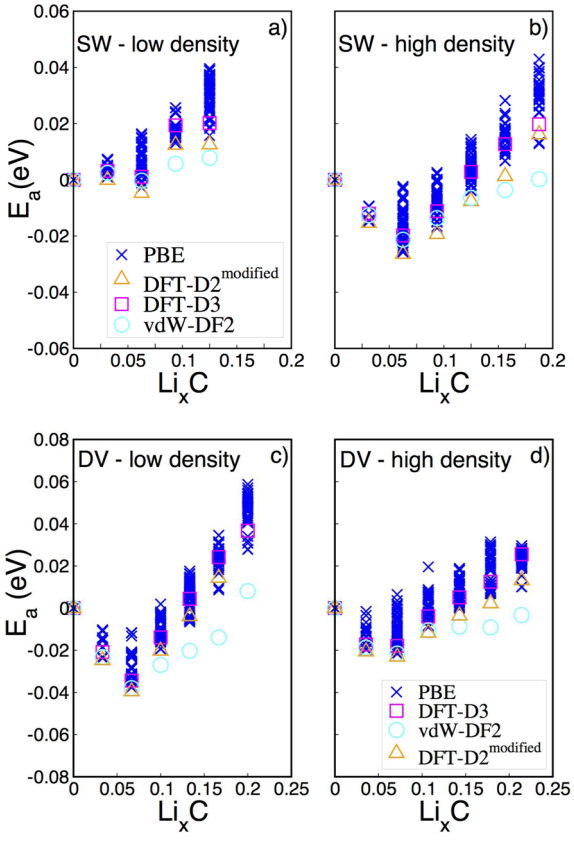

Figure 6. Lithiation energies per C with varying Li content and defect density obtained using PBE and all considered vdW functionals for graphene with (a,b) SW defects and (c,d) DV defects. The molar fraction of Li, x, is defined as $x = n_{Li}/n_C$.

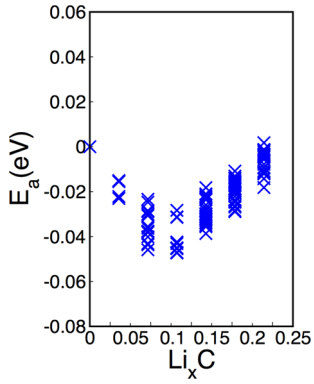

Figure 7. Lithiation energies per C with varying Li content for graphene with an extended defect obtained using PBE. The molar fraction of Li is defined as $x = n_{Li}/n_C$.

At a low density of SW defects (Figure 6a), we find, similar to the pristine graphene, that PBE gives a positive lithiation energy (negative lithiation potential), and the lithiation energy monotonically becomes more positive with Li content, implying zero capacity. With an increase in defect density, as shown in Figure 6b, the lithiation energy has a negative slope for up to two Li (x =0.0625), above which the slope becomes positive. The minimum of the formation energy indicates the Li-saturated composition above which metallic Li precipitation is likely.[44,69] As is evident from the adsorption energy dependence on the composition at higher Li coverages, increasing Li content significantly reduces the adsorption strength with the underlying graphene as a result of increasing Li–Li repulsion. Similarly, the lithiation energies for graphene with low and high density DV defects are shown in Figure 6c,d. For low defect density, Figure 6c, the lithiation energy shows a negative slope for up to two Li (x = 0.067), above which the slope becomes positive, suggesting that metallic Li precipitation is likely. Note that the strength of Li–C interaction for this defect is stronger than that of the SW defect. With increasing defect density, for the less stable DV defect configuration predicted by the GA (Figure 2b), the lithiation energy (Figure 6d) has a negative slope for up to two Li (x = 0.071), and then the slope becomes positive. Comparing the results for two DV defect densities, we find less exothermic Li formation energies for the high density case, corresponding to less positive voltages, although the saturation capacity remains almost unchanged. We note that the weaker binding likely results from the specific defect configurations and will not necessarily be observed for all DV defect arrangements, as shown in the following section on the extended defects.

The above Li/C ratios imply lithiation capacities below that offered by graphite (372 mAh/g). These observations suggest that graphene, at least with the point defects and defect densities discussed above, is unlikely to lead to higher capacity than graphite. This conclusion, in turn, is broadly consistent with a variety of experimental studies. The experimental observations using electrochemical techniques and *in situ* Raman spectroscopy for lithiated SLG and FLG reported by Pollak et al.,[32] show that SLG does not have any sharp anodic and cathodic peaks in the cyclic voltammograms (CV). Li intercalation into graphite, on the other hand, is known to appear as well-defined cathodic peaks associated with the

formation of different intercalation stages (stages 1 and 2)[70] that are also observed for the FLG. *In situ* Raman spectra for SLG showed a gradual shift of the G-band to higher frequency upon cathodic polarization resulting from electron doping. The shift was completed at 0.5 V, and upon polarization at potentials less than 0.5 V, no further shift was observed, suggesting that Li doping reached its maximum level at 0.5 V. The presence of a G-band at 0.01 V for the SLG also ruled out the formation of the LiC_6 phase as seen for the lithiated FLG. Liu et al.[44] suggested that the difference in lithiation behavior between graphene and graphite results from differences in the Li−C binding energies. The more favorable Li intercalation energies in graphite are assigned to charge screening from the multiple graphene layers, which reduces repulsion between intercalated Li ions.[44]

Li Adsorption on Graphene with an Extended Defect. As a final model for lithiation of high defect density graphene, adsorption of varying Li content on graphene with an extended defect (Figure 2a) is evaluated and compared with the less stable high density DV defect configurations discussed above (Figure 2b). The most stable Li adsorption site for the extended defect is on top of the octagon (Figure 5b), with stronger adsorption energy as compared to the less stable high density DV defect (Figure 5c, with an isolated Li adsorption energy difference of 100 meV). As Li is successively adsorbed on graphene with an extended defect, higher Li content configurations will consist of two octagons. This ultimately further enhances Li adsorption on this defect configuration. Indeed, the differential binding energy analysis shows that three Li can be stably adsorbed on the extended defect (x = 0.107), which is higher than the number of Li associated with the other defects considered in this study.

Figure 7 shows the lithiation energy plot as a function of composition. The plot has a negative slope up to a composition of x = 0.107. As compared to the point defect configurations considered, the results show that more Li can be adsorbed on graphene with this one-dimensional extended defect. Although this extended defect is made of point defects as the building blocks, and it has the same density as the case with two DV defect in the cell (Figure 2b), the fact that the initial Li adsorption is more favorable for the extended defect allows enhanced adsorption upon successive lithiation. This special configuration of the octagons in an extended defect seems promising for increasing the capacity as compared to the considered defect configurations here. It has been shown that CVD-grown graphene on a Ni(111) substrate accommodates such one-dimensional extended defects embedded into the hexagonal graphene lattice.[51]

Enhanced Capacities for Graphene with Defects. Using the results of the maximum percentage of Li adsorbed stably on graphene with varying defect densities (corresponding both to the transition from positive to negative differential binding energies and to the composition at the minimum of the formation energy plots), we calculate the corresponding capacities, C (mAh/g). As mentioned above, for both pristine graphene and graphene with low densities of SW defects, Li does not adsorb stably, and hence, for both structures, the capacity is zero. In contrast, for graphene with low density DV defects, we find that the maximum Li adsorption is ∼6.7%, giving a capacity of 149 mAh/g for Li. The result suggests that graphene with one DV defect could in fact turn pristine graphene into an anode of modest capacity. The calculated capacity for Li on the graphene with DV defects is lower than that for the bilayer graphene[33,44] (186 mAh/g) and that offered by graphite (372 mAh/g).[5,33,44] Increasing the density of the SW defects makes it possible for Li to be adsorbed with a maximum concentration of 6.25%. The corresponding capacity is 140 mAh/g, which is again lower than that offered by the bilayer graphene and the graphite.[33,44] The maximum percentage of Li adsorption on the high density DV defect is 7.1%, which in turn gives a capacity of 159 mAh/g. On the other hand, graphene with an extended defect shows the maximum Li adsorption to be 10.7%, giving a capacity on the order of 239 mAh/g. This result suggests that the extended defect configuration could enhance the capacity, storing more Li as compared to the point defects considered here, and compared to the bilayer graphene reported in earlier studies.[33,44] It is possible that, by carefully engineering extended defects of even higher density into graphene, electrodes with capacities approaching that of graphite might ultimately be developed.

4. CONCLUSIONS

First-principles calculations are performed to explore Li adsorption on pristine SLG, SLG with varying densities of SW and DV point defects, and an extended defect. Accordingly, the effectiveness of the modified graphene structures for Li storage is evaluated. The most stable adsorption sites for Li in all structures are the hollow sites on the defect zones. The defect zones, in turn, have a tendency to capture Li with stronger adsorption in these regions. For high Li coverages, the lowest energy adsorption configurations are associated with Li being adsorbed on both sides of the graphene sheet. The results for Li adsorption on pristine SLG are in agreement with earlier observations that on defect-free SLG, Li has a positive adsorption energy, which monotonically increases with increasing Li content. For graphene with low density SW defects, the Li adsorption energy is positive as well, suggesting that both defect-free SLG and graphene with low density SW defects are unsuitable for storing Li. On the other hand, Li adsorption is relatively strong on the DV defects with an adsorption energy magnitude of 0.71 eV. The inclusion of vdW interactions has a minimal effect on the determined trends compared to standard PBE calculations.

Based on the analysis of the most stable compositions, the calculated capacities suggest that for point defects, increasing density of SW defects make it possible to reach a capacity on the order of 140 mAh/g, which is a significant enhancement in comparison to the lower density SW defects (zero capacity). The presence of DV defects on graphene leads to modest capacities of up to 160 mAh/g, which is, however, still lower than that of graphite. The analysis of an extended defect on graphene suggests that the presence of such extended defects could lead to much higher capacities (240 mAh/g) than those of the point defects, as well as of those of the bilayer graphene; however, the capacities are still below those of graphite. Although the overall predicted capacities are still modest, these results support the potential interest in engineering graphene with defects to activate the graphene surfaces for achieving enhanced Li capacities in LIBs. We suggest that further increasing the densities of extended defects may potentially help to improve the capacity, and even perhaps ultimately exceed the capacity of graphite if suitable defect configurations can be tailored.

■ ASSOCIATED CONTENT

Supporting Information

Technical details about the genetic algorithm as well as the results regarding the structure of the lowest energy adsorption configurations of Li are given. The defect formation energies and Li adsorption energies are reported for larger cell sizes. This material is available free of charge via the Internet at http://pubs.acs.org.

■ AUTHOR INFORMATION

Corresponding Author

*J. P. Greeley. E-mail: jgreeley@purdue.edu.

Notes

The authors declare no competing financial interest.

■ ACKNOWLEDGMENTS

This research was supported as part of the Center for Electrochemical Energy Science, an Energy Frontier Research Center funded by the U.S. Department of Energy, Office of Science, Office of Basic Energy Sciences. Use of the Center for Nanoscale Materials was supported by the U.S. Department of Energy, Office of Science, Office of Basic Energy Sciences, under Contract No. DE-AC02-06CH11357. Computational resources provided by the National Energy Research Scientific Computing Center (NERSC) are gratefully acknowledged.

■ REFERENCES

(1) Tarascon, J. M.; Armand, M. Issues and Challenges Facing Rechargeable Lithium Batteries. *Nature* **2001**, *414*, 359−367.

(2) Bruce, P. G.; Scrosati, B.; Tarascon, J.-M. Nanomaterials for Rechargeable Lithium Batteries. *Angew. Chem., Int. Ed.* **2008**, *47*, 2930−2946.

(3) Ceder, G.; Hautier, G.; Jain, A.; Ong, S. P. Recharging Lithium Battery Research with First-Principles Methods. *MRS Bull.* **2011**, *36*, 185−191.

(4) Goodenough, J. B.; Park, K.-S. The Li-Ion Rechargeable Battery: A Perspective. *J. Am. Chem. Soc.* **2013**, *135*, 1167−1176.

(5) Winter, M.; Besenhard, J. O.; Spahr, M. E.; Novak, P. Insertion Electrode Materials for Rechargeable Lithium Batteries. *Adv. Mater.* **1998**, *10*, 725−763.

(6) Kasuh, T.; Mabuchi, A.; Tokumitsu, K.; Fujimoto, H. Recent Trends in Carbon Negative Electrode Materials. *J. Power Sources* **1997**, *68*, 99−101.

(7) Azuma, H.; Imoto, H.; Yamada, S.; Sekai, K. Advanced Carbon Anode Materials for Lithium Ion Cells. *J. Power Sources* **1999**, *81*, 1−7.

(8) Noel, M.; Suryanarayanan, V. Role of Carbon Host Lattices in Li-Ion Intercalation/De- intercalation Processes. *J. Power Sources* **2002**, *111*, 193−209.

(9) Burkhardt, S. E.; Bois, J.; Tarascon, J.-M.; Hennig, R. G.; Abrunna, H. D. Li-Carboxylate Anode Structure-Property Relationships from Molecular Modeling. *Chem. Mater.* **2013**, *25*, 132−141.

(10) Pistoia, G. *Lithium Batteries: New Materials, Developments, and Perspectives*, 2nd ed; Elsevier Science Publishers: Amsterdam, 1994.

(11) Novoselov, K. S.; Geim, A. K.; Morozov, S. V.; Jiang, D.; Zhang, Y.; Dubonos, S. V.; Grigorieva, I. V.; Firsov, A. A. Electric Field Effect in Atomically Thin Carbon Films. *Science* **2004**, *306*, 666−669.

(12) Neto, A. H. C.; Guinea, F.; Peres, N. M. R.; Novoselov, K. S.; Geim, A. K. The Electronic Properties of Graphene. *Rev. Mod. Phys.* **2009**, *81*, 109.

(13) Patchkovskii, S.; Tse, J. S.; Yurchenko, S. N.; Zhechkov, L.; Heine, T.; Seifert, G. Graphene Nanostructures as Tunable Storage Media for Molecular Hydrogen. *Proc. Natl. Acad. Sci. U. S. A.* **2005**, *102*, 10439−10444.

(14) Yoo, E.; Kim, J.; Hosono, E.; Zhou, H.-S.; Kudo, T.; Honma, I. Large Reversible Li Storage of Graphene Nanosheet Families for Use in Rechargeable Lithium Ion Batteries. *Nano Lett.* **2008**, *8*, 2277−2282.

(15) Jang, B. Z.; Liu, C.; Neff, D.; Yu, Z.; Wang, M. C.; Xiong, W.; Zhamu, A. Graphene Surface-Enabled Lithium Ion-Exchanging Cells: Next-Generation High-Power Energy Storage Devices. *Nano Lett.* **2011**, *11*, 3785−3791.

(16) Wang, G.; Shen, X.; Yao, J.; Park, J. Graphene Nanosheets for Enhanced Lithium Storage in Lithium Ion Batteries. *Carbon* **2009**, *47*, 2049−2053.

(17) Kaskhedikar, N. A.; Maier, J. Lithium Storage in Carbon Nanostructures. *Adv. Mater.* **2009**, *21*, 2664−2680.

(18) Yoo, E.-J.; Jedeok, K.; Hosono, E.; Zhou, H.-S.; Kudo, T.; Honma, I. Large Reversible Li Storage of Graphene Nanosheet Families for Use in Rechargeable Lithium Ion Batteries. *Nano Lett.* **2008**, *8*, 2277−2282.

(19) Zhou, M.; Cai, T.; Pu, F.; Chen, H.; Wang, Z.; Zhang, H.; Guan, S. Graphene/Carbon- Coated Si Nanoparticle Hybrids as High-Performance Anode Materials for Li-Ion Batteries. *ACS Appl. Mater. Interfaces* **2013**, *5*, 3449−3455.

(20) Wu, P.; Wang, H.; Tang, Y.; Zhou, Y.; Lu, T. Three-Dimensional Interconnected Network of Graphene-Wrapped Porous Silicon Spheres: In Situ Magnesiothermic-Reduction Synthesis and Enhanced Lithium-Storage Capabilities. *ACS Appl. Mater. Interfaces* **2014**, *6*, 3546−3552.

(21) Xu, C.; Xu, B.; Gu, Y.; Xiong, Z.; Sun, J.; Zhao, X. S. Graphene-based Electrodes for Electrochemical Energy Storage. *Energy Environ. Sci.* **2013**, *6*, 1388−1414.

(22) Ren, J.-G.; Wu, Q.-H.; Tang, H.; Hong, G.; Zhang, W.; Lee, S.-T. Germanium−Graphene Composite Anode for High-Energy Lithium Batteries with Long Cycle Life. *J. Mater. Chem. A* **2013**, *1*, 1821−1826.

(23) Pan, D.; Wang, S.; Zhao, B.; Wu, M.; Zhang, H.; Wang, Y.; Jiao, Z. Li Storage Properties of Disordered Graphene Nanosheets. *Chem. Mater.* **2009**, *21*, 3136−3142.

(24) Lian, P.; Zhu, X.; Liang, S.; Li, Z.; Yang, W.; Wang, H. Large Reversible Capacity of High Quality Graphene Sheets as an Anode Material for Lithium-Ion Batteries. *Electrochim. Acta* **2010**, *55*, 3909−3914.

(25) Dahn, J. R.; Zheng, T.; Liu, Y.; Xue, J. S. Mechanisms for Lithium Insertion in Carbonaceous Materials. *Science* **1995**, *270*, 590−593.

(26) Medeiros, P. V. C.; de Brito Mota, F.; Mascarenhas, A. J. S.; de Castilho, C. M. C. Adsorption of Monovalent Metal Atoms on Graphene: A Theoretical Approach. *Nanotechnology* **2010**, *21*, 115701.

(27) Yang, C.-K. A Metallic Graphene Layer Adsorbed with Lithium. *Appl. Phys. Lett.* **2009**, *94*, 163115.

(28) Chan, K. T.; Neaton, J. B.; Cohen, M. L. First-Principles Study of Metal Adatom Adsorption on Graphene. *Phys. Rev. B* **2008**, *77*, 235430.

(29) Khantha, M.; Cordero, N. A.; Molina, L. M.; Alonso, J. A.; Girifalco, L. A. Interaction of Lithium with Graphene: An *Ab Initio* Study. *Phys. Rev. B* **2004**, *70*, 125422.

(30) Zheng, J.; Ren, Z.; Guo, P.; Fang, L.; Fan, J. Diffusion of Li^+ Ion on Graphene: A DFT study. *Appl. Surf. Sci.* **2011**, *258*, 1651−1655.

(31) Li, J.; Wu, C.; Guan, L. Lithium Insertion/Extraction Properties of Nanocarbon Materials. *J. Phys. Chem. C* **2009**, *113*, 18431−18435.

(32) Pollak, E.; Geng, B.; Jeon, K.-J.; Lucas, I. T.; Richardson, T. J.; Wang, F.; Kostecki, R. The Interaction of Li^+ with Single-Layer and Few-Layer Graphene. *Nano Lett.* **2010**, *10*, 3386−3388.

(33) Lee, E.; Persson, K. A. Li Absorption and Intercalation in Single Layer Graphene and Few Layer Graphene by First Principles. *Nano Lett.* **2012**, *12*, 4624−4628.

(34) Tachikawa, H.; Nagoya, Y.; Fukuzumi, T. Density Functional Theory (DFT) Study on the Effects of Li^+ Doping on Electronic States of Graphene. *J. Power Sources* **2010**, *195*, 6148−6152.

(35) Ataca, C.; Aktürk, E.; Ciraci, S.; Ustunel, H. High-Capacity Hydrogen Storage by Metallized Graphene. *Appl. Phys. Lett.* **2008**, *93*, 043123.

(36) Valencia, F.; Romero, A. H.; Anciloto, F.; Silvestrelli, P. L. Lithium Adsorption on Graphite from Density Functional Theory Calculations. *J. Phys. Chem. B* **2006**, *110*, 14832−14841.
(37) Garay-Tapia, A. M.; Romero, A. H.; Barone, V. Lithium Adsorption on Graphene: From Isolated Adatoms to Metallic Sheets. *J. Chem. Theory Comput.* **2012**, *8*, 1064−1071.
(38) Fan, X.; Zheng, W. T.; Kuo, J.-L.; Singh, D. J. Adsorption of Single Li and the Formation of Small Li Clusters on Graphene for the Anode of Lithium-Ion Batteries. *ACS Appl. Mater. Interfaces* **2013**, *5*, 7793−7797.
(39) Zheng, J.; Ren, Z.; Guo, P.; Fang, L.; Fan, J. Diffusion of Li^+ Ion on Graphene: A DFT Study. *Appl. Surf. Sci.* **2011**, *258*, 1651−1655.
(40) Tachikawa, H. A Direct Molecular Orbital−Molecular Dynamics Study on the Diffusion of the Li Ion on a Fluorinated Graphene Surface. *J. Phys. Chem. C* **2008**, *112*, 10193−10199.
(41) Tachikawa, H.; Shimizu, A. Diffusion Dynamics of the Li Atom on Amorphous Carbon: A Direct Molecular Orbital−Molecular Dynamics Study. *J. Phys. Chem. B* **2006**, *110*, 20445−20450.
(42) Yao, F.; Güneş, F.; Ta, H. Q.; Lee, S. M.; Chae, S. J.; Sheem, K. Y.; Cojocaru, C. S.; Xie, S. S.; Lee, Y. H. Diffusion Mechanism of Lithium Ion through Basal Plane of Layered Graphene. *J. Am. Chem. Soc.* **2012**, *134*, 8646−8654.
(43) Fan, X.; Zheng, W. T.; Kuo, J.-L. Adsorption and Diffusion of Li on Pristine and Defective Graphene. *ACS Appl. Mater. Interfaces* **2012**, *4*, 2432−2438.
(44) Liu, Y.; Artyukhov, V. I.; Liu, M.; Harutyunyan, A. R.; Yakobson, B. I. Feasibility of Lithium Storage on Graphene and Its Derivatives. *J. Phys. Chem. Lett.* **2013**, *4*, 1737−1742.
(45) Hashimoto, A.; Suenaga, K.; Gloter, A.; Urita, K.; Iijima, S. Direct Evidence for Atomic Defects in Graphene Layers. *Nature* **2004**, *430*, 870−873.
(46) Gass, M. H.; Bangert, U.; Bleloch, A. L.; Wang, P.; Nair, R. R.; Geim, A. K. Free-Standing Graphene at Atomic Resolution. *Nat. Nanotechnol.* **2008**, *3*, 676−681.
(47) Meyer, J. C.; Kisielowski, C.; Erni, R.; Rossell, M. D.; Crommie, M. F.; Zettl, A. Direct Imaging of Lattice Atoms and Topological Defects in Graphene Membranes. *Nano Lett.* **2008**, *8*, 3582−3586.
(48) Kotakoski, J.; Krasheninnikov, A. V.; Kaiser, U.; Meyer, J. C. From Point Defects in Graphene to Two-Dimensional Amorphous Carbon. *Phys. Rev. Lett.* **2011**, *106*, 105505.
(49) Ugeda, M. M.; Brihuega, I.; Guinea, F.; Gomez-Rodriguez, J. M. Missing Atom as a Source of Carbon Magnetism. *Phys. Rev. Lett.* **2010**, *104*, 096804.
(50) Tapaszto, L.; Dobrik, G.; Nemes-Incze, P.; Vertesy, G.; Lambin, P.; Biro, L. P. Tuning the Electronic Structure of Graphene by Ion Irradiation. *Phys. Rev. B* **2008**, *78*, 233407.
(51) Lahiri, J.; Lin, Y.; Bozkurt, P.; Oleynik, I. I.; Batzill, M. An Extended Defect in Graphene as a Metallic Wire. *Nat. Nanotechnol.* **2010**, *5*, 326−329.
(52) Rodrıguez-Manzo, J. A.; Banhart, F. Creation of Individual Vacancies in Carbon Nanotubes by Using an Electron Beam of 1 A Diameter. *Nano Lett.* **2009**, *9*, 2285−2289.
(53) Hohenberg, P.; Kohn, W. Inhomogeneous Electron Gas. *Phys. Rev.* **1964**, *136*, B864.
(54) Kresse, G.; Furthmüller, J. Efficient Iterative Schemes for *Ab Initio* Total-Energy Calculations Using a Plane-Wave Basis Set. *Phys. Rev. B* **1996**, *54*, 11169.
(55) Perdew, J. P.; Burke, K.; Ernzerhof, M. Generalized Gradient Approximation Made Simple. *Phys. Rev. Lett.* **1996**, *77*, 3865.
(56) Stone, A. J.; Wales, D. Theoretical Studies of Icosahedral C_{60} and Some Related Species. *J. Chem. Phys. Lett.* **1986**, *128*, 501−503.
(57) Grimme, S. Semiempirical GGA-Type Density Functional Constructed with a Long-Range Dispersion Correction. *J. Comput. Chem.* **2006**, *27*, 1787−1799.
(58) Grimme, S.; Antony, J.; Ehrlich, S.; Krieg, S. A Consistent and Accurate *Ab Initio* Parametrization of Density Functional Dispersion Correction (DFT-D) for the 94 Elements H-Pu. *J. Chem. Phys.* **2010**, *132*, 154104.
(59) Lee, K.; Murray, E. D.; Kong, L.; Lundqvist, B. I.; Langreth, D. C. Higher-Accuracy van der Waals Density functional. *Phys. Rev. B* **2010**, *82*, 081101.
(60) Klimeš, J.; Bowler, D. R.; Michaelides, A. Chemical Accuracy for the van der Waals Density Functional. *J. Phys.: Condens. Matter* **2010**, *22*, 022201.
(61) Klimeš, J.; Bowler, D. R.; Michaelides, A. van der Waals Density Functionals Applied to Solids. *Phys. Rev. B* **2011**, *83*, 195131.
(62) Lusk, M. T.; Carr, L. D. Nanoengineering Defect Structures on Graphene. *Phys. Rev. Lett.* **2008**, *100*, 175503.
(63) Ma, J.; Alfe, D.; Michaelides, A.; Wang, E. Stone-Wales Defects in Graphene and Other Planar sp^2-Bonded Materials. *Phys. Rev. B* **2009**, *80*, 033407.
(64) Mehmood, F.; Pachter, R.; Lu, W.; Boeckl, J. Adsorption and Diffusion of Oxygen on Single-Layer Graphene with Topological Defects. *J. Phys. Chem. C* **2013**, *117*, 10366−10374.
(65) Fan, X. F.; Zheng, W. T.; Chihaia, V.; Shen, Z. X.; Kuo, J.-L. Interaction between Graphene and the Surface of SiO_2. *J. Phys.: Condens. Matter* **2012**, *24*, 305004.
(66) Graziano, G.; Klimeš, J.; Fernandez-Alonso, F.; Michaelides, A. Improved Description of Soft Layered Materials with van der Waals Density Functional Theory. *J. Phys.: Condens. Matter* **2012**, *24*, 424216.
(67) Henkelman, G.; Arnaldsson, A.; Jonsson, H. A Fast and Robust Algorithm for Bader Decomposition of Charge Density. *Comput. Mater. Sci.* **2006**, *36*, 354−360.
(68) Persson, K.; Hinuma, Y.; Meng, Y. S.; Van der Ven, A.; Ceder, G. Thermodynamic and Kinetic Properties of the Li-Graphite System from First-Principles Calculations. *Phys. Rev. B* **2010**, *82*, 125416.
(69) Chan, M. K. Y.; Wolverton, C.; Greeley, J. P. First Principles Simulations of the Electrochemical Lithiation and Delithiation of Faceted Crystalline Silicon. *J. Am. Chem. Soc.* **2012**, *134*, 14362−14374.
(70) Aurbach, D.; Markovsky, B.; Weissman, I.; Levi, E.; Ein-Eli, Y. On the Correlation Between Surface Chemistry and Performance of Graphite Negative Electrodes for Li Ion Batteries. *Electrochim. Acta* **1999**, *45*, 67−86.